Co-optimizing grating couplers for hybrid integration of InP and SOI photonic platforms

M. Passoni, F. Floris, H. Y. Hwang, L. Zagaglia, L. Carroll, L. C. Andreani, and P. O'Brien

Citation: AIP Advances **8**, 095109 (2018); doi: 10.1063/1.5046164
View online: https://doi.org/10.1063/1.5046164
View Table of Contents: http://aip.scitation.org/toc/adv/8/9
Published by the American Institute of Physics

Co-optimizing grating couplers for hybrid integration of InP and SOI photonic platforms

M. Passoni,[1,2,a] F. Floris,[1] H. Y. Hwang,[1] L. Zagaglia,[1] L. Carroll,[1]
L. C. Andreani,[2] and P. O'Brien[1]
[1]*Photonic Packaging Group, Tyndall National Institute, T12R5CP Cork, Ireland*
[2]*Department of Physics, University of Pavia, 27100 Pavia, Italy*

(Received 26 June 2018; accepted 3 September 2018; published online 14 September 2018)

Grating couplers are widely used optical interfaces in integrated photonics, especially on the Silicon-On-Insulator (SOI) platform. Their design has been optimized for coupling light between a Photonic Integrated Circuit (PIC) and a single-mode fiber, a μlens for free space transport, or even a second PIC in the same SOI platform. In this work, we co-design matching pairs of grating-couplers on distinct SOI and InP photonic platforms for optimized PIC-to-PIC coupling. By matching the scattering strengths of the two grating-couplers, we show that a PIC-to-PIC insertion loss of 3dB can be achieved. We also investigate how the design parameters impact the coupling efficiency and the bandwidth, ending up with a tolerance analysis. The proposed coupling approach between two different waveguide materials has prospective applications for the hybrid-integration of SOI and InP photonic platforms for communication technologies. https://doi.org/10.1063/1.5046164

I. INTRODUCTION

Optimizing Fiber-to-PIC coupling has been a major research topic in the photonics community during the last two decades. Various approaches have been investigated including edge-coupling, evanescent-coupling, and grating-based coupling. The latter option offers relaxed alignment tolerances that allow for low-cost Fiber-to-PIC packaging with multi-channel fiber arrays for high-capacity datacom and telecom devices.[1] Grating-couplers on the SOI platform benefit from a high index-contrast that offers a strong light-matter interaction over the 10 μm mode-field diameter (MFD) of a standard single-mode fiber — see Fig. 1(a). Many different grating-coupler designs have been proposed to optimize Fiber-to-PIC coupling performance for specific applications.[2–7] Recently, grating-couplers have found applications beyond Fiber-to-PIC coupling, such as for vertical PIC-to-PIC coupling between stacked SOI-PICs — see Fig. 1(b) — or for inter-layer coupling within the same PIC.[8,9] While PIC-to-PIC coupling between an identical pair of grating-couplers on matching SOI-PICs has already been demonstrated, design of efficient PIC-to-PIC coupling between InP and SOI is a much more complex problem that is tackled in this work by co-designing the two different gratings, see sketch in Fig. 1(c). A grating-coupler approach for the hybrid integration of these two key photonic platforms brings advantages over competing technologies like wafer-to-wafer bonding[10] (which can suffer from low-yield, and significant material wastage) and transfer-printing[11] (which requires sub-μm alignment tolerances). The approach proposed here can be used to integrate III-V lasers and semiconductor optical amplifiers (SOAs) on the indirect band-gap SOI-platform, in order to reach increased photonic functionality and compensation of interface and transmission losses.[12,13]

[a]marco.passoni01@ateneopv.it

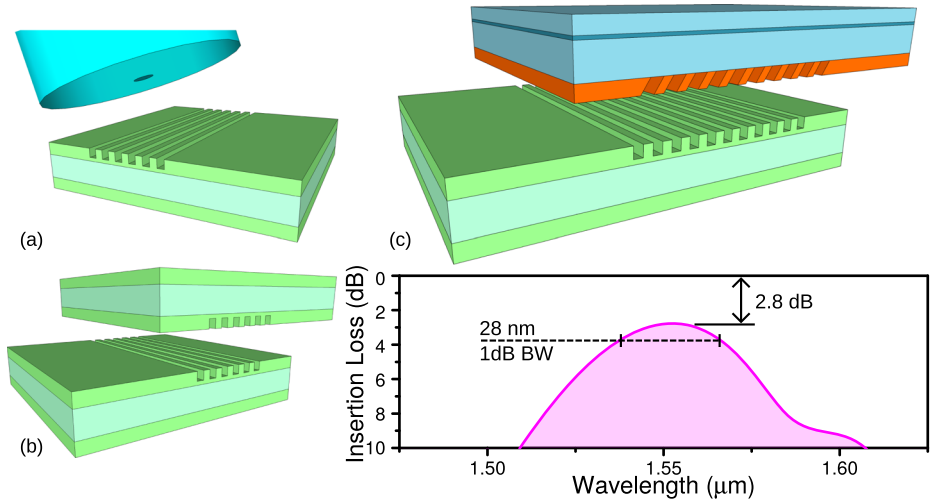

FIG. 1. Two known applications of grating-couplers: fiber-to-chip (a), and chip-to-chip (SOI) (b). Our proposed application, SOI chip to InP chip, and related insertion loss for the best structure with grating length 150 μm (c).

The index-contrast of the SOI-platform is high (n=3.48 for Si, and n=1.44 for SiO_2 at 1550 nm), therefore even partially etched SOI grating-couplers have a scattering-strength that can be well-matched to the 10.4 μm MFD of a standard SMF28 single-mode fiber. However, the index-contrast of the InP-platform is significantly lower, because the waveguide (n=3.36) and cladding layers (n=3.17) are both based on InP and differ only by Fe-doping. As a result, the scattering-strength of even a fully-etched InP grating-coupler — see Fig. 2 — is approximately one order-of-magnitude less than that of SOI grating-couplers, resulting in a relatively low Fiber-to-PIC coupling to SMF28 because of the poor modal overlap. Nonetheless, InP grating-couplers can still achieve significant vertical (upward) emission, provided their length is increased sufficiently — see Fig. 3 — to increase the number of scattering sites, i.e., the number of grating periods. After suitable co-design of both InP and SOI (linearly-chirped) grating-couplers, to best match their scattering-strengths and lengths,

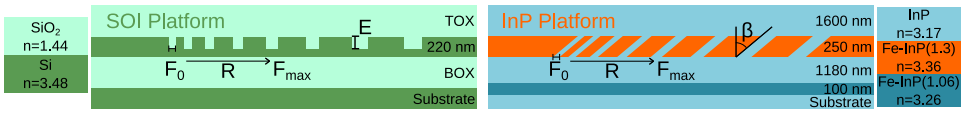

FIG. 2. Sketch of the two platforms under consideration. When a number is provided the parameter is considered fixed, otherwise it is varied in the calculations of this work. Moreover, etching in the InP platform can be performed at a specified (blaze) angle β.

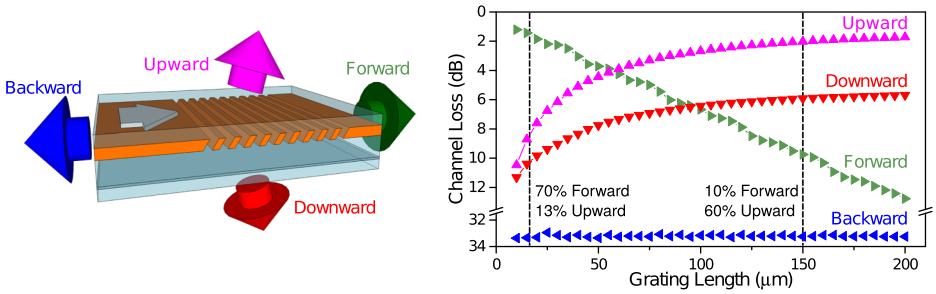

FIG. 3. Analysis of the scattering power of the InP grating. The graph shows how light entering the grating from the waveguide is split in each of the relevant output channels (forward, backward, downward and upward emission) as a function of grating length.

we show — see Fig. 1(c) — that a PIC-to-PIC insertion loss of 2.8 dB (52%), with a 1dB spectral bandwidth of 28 nm, is achievable.

II. SCATTERING-STRENGTH ANALYSIS

In order to co-design the paired grating-coupler system for efficient PIC-to-PIC transfer, a careful analysis of the scattering power of the InP grating is required. We first identify the design parameters for the uniform InP grating that give the maximum scattering strength at 1550 nm. We impose the boundary conditions in terms of layer-composition, -thickness, and -ordering that are available from the multi-project wafer (MPW) integrated-photonic foundry service offered by HHI[14] — see Fig. 2. The largest scattering-strength for a uniform InP grating is achieved with a fill-factor F (the ratio between the etched part and the period) of 0.45, and a blaze-angle β of 50°. Figure 3 shows how light incident from the waveguide on this grating-coupler is distributed across its "Forward", "Backward", "Downward", and "Upward" output channels, as a function of the grating-coupler length L from 10 to 200 μm. As expected for a weakly-scattering system, the fraction of power emitted "Forward" (i.e., across the grating-coupler) exhibits an exponentially decay as a function of distance, with an attenuation loss of 0.06 dB/μm. The fraction of power emitted "Backward" (i.e., reflected back into the waveguide) is less than 30 dB, indicating that feedback effects into integrated gain-components, such as integrated SOAs and lasers, would be manageable.[13] The fraction of power emitted "Upward", where it is available for vertical-coupling purposes, reaches 1.7dB for InP grating-coupler designs with L = 150-200 μm.

The fraction of power emitted "Downward" is still appreciable, since the vertical InP structure is not specifically optimized for upward emission. The directionality, namely the fraction of power emitted upward over the total emitted power, increases with length up to a maximum of 72%, leaving margins for further improvement.

III. GRATING-COUPLERS DESIGN

We optimize both SOI and InP grating-couplers with varying lengths. Beyond the standard 15 μm length used for fiber coupling, we analyze the additional lengths 25, 50, 100, and 150 μm. Greater lengths are not explored since the computational effort in terms of FDTD simulation time becomes prohibitive, while is not expected to lead to appreciable performance gain.

The gratings are placed one above the other, with an air gap of 25 μm between them. This distance is compatible with standard flip-chip technology and ensures the actual coupling mechanism to be waveguide to free-space to waveguide coupling, instead of direct grating-to-grating adiabatic coupling. Notice that for such large distances, beam divergence is an important effect that is taken into account by the FDTD simulations.

A full (brute-force) optimization of the composite grating-coupler system could be interesting, however it has two main drawbacks. The first is due to its intrinsic difficulty, as both grating-couplers have to be tuned to emit/absorb light at the same angle. Moreover, it may not allow to clarify the underlying physics. Our strategy is to separately optimize the grating-couplers, and then to build the composite system using the already developed designs. To ensure good performance when both grating-couplers are brought together, we optimize them as in-coupler devices employing the same input profile, namely a gaussian mode incident from air at an angle $\theta = 14.5°$, at λ=1550 nm and with a Mode Field Diameter (MFD) equal to L — see Fig. 4.

The optimization procedure resorts to a variation of the design rule developed by Marchetti *el al.*[7] for apodized SOI grating-couplers. This approach is able to provide a compact representation of a linearly-chirped grating-coupler depending only on two parameters, namely the initial fill-factor F_0 and the apodization coefficient R. The numerical optimization is then carried out with a standard Particle Swarm Optimization (PSO) algorithm,[15] run with 10 agents and 150 iterations for each configuration. Simulations are performed with the 2D FDTD method using the commercial software Lumerical FDTD Solutions (from *Lumerical Inc.*).

Nevertheless, we make two modifications to the design rule: first, we establish a maximum fill-factor F_{max}, and second, we introduce a corrective coefficient a in setting the period. The maximum fill-factor is simply introduced for numerical reasons: it forbids the fill-factor $F(x)$ to become greater

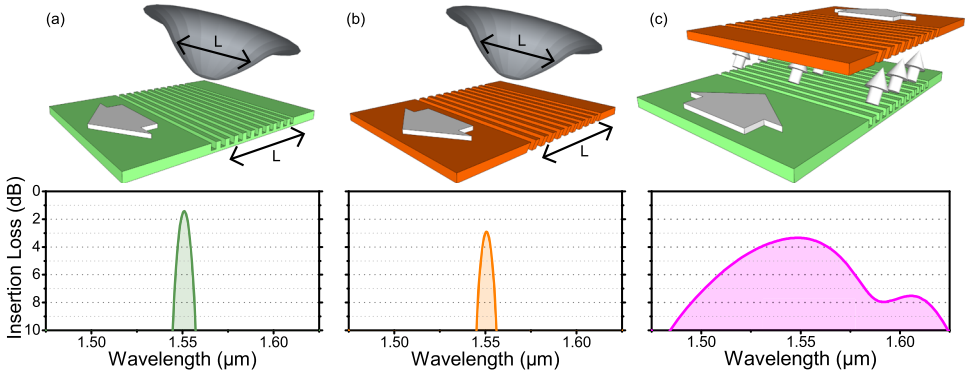

FIG. 4. Upper panels: graphical illustration of our strategy to build the PIC to PIC configuration. Both SOI (a) and InP (b) gratings are separately optimized as in-couplers with an appropriate gaussian excitation, then joined together (c). Lower panels: examples of coupling spectra for the 100 μm long gratings.

than one, allowing a smooth functioning of the PSO algorithm for arbitrarily long gratings. The evolution of the fill-factor with the position x along the chirped grating is given by:

$$F(x) = \min(F_0 + Rx, F_{max}). \tag{1}$$

The local period Λ is then adjusted with the Bragg condition, to make sure that each section of the grating is precisely tuned in both wavelength λ and angle θ:

$$\Lambda(x) = a\frac{\lambda}{n_e(x) - \sin(\theta)}. \tag{2}$$

The a parameter is here inserted to compensate for the mismatch in the Bragg-condition introduced by the approximate estimation of n_e,[7] and selected with an iterative tuning procedure.

The optimization parameters of the InP grating-coupler are thus F_0, F_{max}, R, and β. The vertical structure is fixed and full etch of the Fe-doped InP layer is chosen in order to maximize the scattering strength. The equivalent parameters for the SOI grating are F_0, F_{max}, and R, and in addition E, T, and B, which are the etching depth and the thicknesses of the TOX and BOX layers, respectively. We consider a variable etching depth E in the SOI grating, because reducing its value is the most straightforward way to decrease the scattering power.[16] See Fig. 2 for the complete definitions of parameters.

A performance summary of the PIC-to-PIC configurations for the optimized gratings is shown in Fig. 5, where the insertion loss and the 1dB-bandwidth are reported as a function of grating length. We observe an improvement in insertion loss on increasing the grating length. Moreover, the bandwidth decreases on increasing length,[16] although its absolute value remains greater than or comparable to the typical bandwidth of a fiber-to-PIC scheme. A total insertion loss of 2.8 dB can be reached using

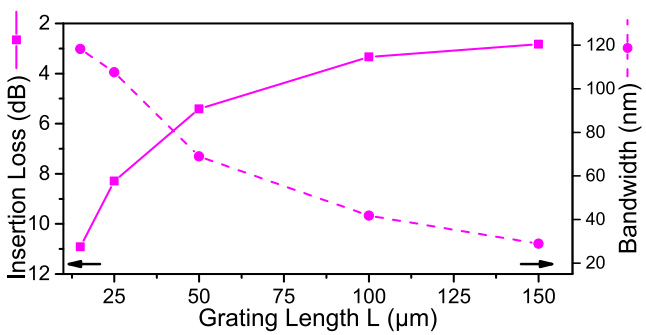

FIG. 5. Performances as a function of grating length for the optimized PIC-to-PIC configuration. The trade-off between insertion loss and bandwidth of the structure is clearly apparent.

TABLE I. Parameters of the SOI grating.

Length (μm)	E (nm)	F_0	F_{max}	R (m^{-1})	B (μm)	T (μm)	$100(a-1)$
15	110	0.1	1.0	27500	2.00	0.72	0.00[7]
25	85	0.1	0.59	9925	1.97	0.21	0.417
50	53	0.1	0.57	6552	1.95	0.24	0.052
100	35	0.1	0.53	4276	1.93	0.25	-0.035
150	30	0.1	0.55	2198	1.93	0.25	0.024

TABLE II. Parameters of the InP grating.

Length (μm)	F_0	F_{max}	R (m^{-1})	β (deg)	$100(a-1)$
15	0.38	1.0	5387	49	-0.741
25	0.37	0.55	5020	51	-0.756
50	0.39	0.44	4753	50	-0.674
100	0.36	0.42	2449	54	-0.725
150	0.36	0.40	1375	57	-0.775

a 150 μm long grating configuration — see Fig. 1(c). Shorter structures may be useful if a small reduction in coupling efficiency could be accepted in order to have a more compact or broadband device. Each PIC-to-PIC configuration is simulated considering operation in both directions, showing no practical difference in the coupling spectrum.

The main sources of loss, up to ≈ 2dB, are the losses to both substrates. The most straightforward way to reduce them is to optimize the layer thicknesses of the InP grating. The present vertical structure (see Fig. 2), which was kept fixed for compatibility with HHI platform, is indeed sub-optimal for this kind of application. Thus, a complete optimization of the InP grating, taking into account also the vertical structure, could improve directionality and ultimately reduce the total insertion loss.

The parameters of the optimized structures are reported in Table I (SOI) and II (InP). These parameters have a relatively small variation with the length of the grating, except for the apodization coefficient R and the etch depth E in the silicon grating. This is quite reasonable since the aim of the InP grating is to increase the total scattering-power as much as possible, thus the optimization always converges to the grating configuration yielding the maximum scattering-strength. For the SOI grating the opposite is true, the total scattering-power is held constant and the scattering-strength has to be reduced to compensate for the increase in the number of scatterers. Starting from a perfect vertical overlap between the two gratings, a sweep over horizontal offset values shows that the optimal configuration for the PIC-to-PIC is achieved when a small shift (~ 3-5 μm) is applied. The tolerance on this parameter is however very relaxed: the 1dB alignment tolerance is 6 μm in the worst case (for 15 μm long gratings), and much higher for the longer grating-couplers.

IV. FAR-FIELD ANALYSIS

To gain an insight on the physical reasons behind the trends in Fig. 5, we now study the output profiles of both grating-couplers in the far-field. Since their emission and acceptance features basically coincide, the far-field profile indicates how well the emission of one grating is tailored to the acceptance of the other. In Fig. 6 we display the far-field profiles (as a function of angle and wavelength) of both SOI- and InP-gratings for the two lengths L = 25 and 150 μm. The region in which the two profiles overlap indicates where the coupling takes place.

The far-field profile related to the shorter gratings has relatively wide peaks: the overlap region basically spans all the interesting wavelengths, therefore justifying the broadband behavior. On the contrary, the far-field profile relative to the longer gratings has narrower peaks, the width of the overlap region is reduced, and so is the bandwidth.

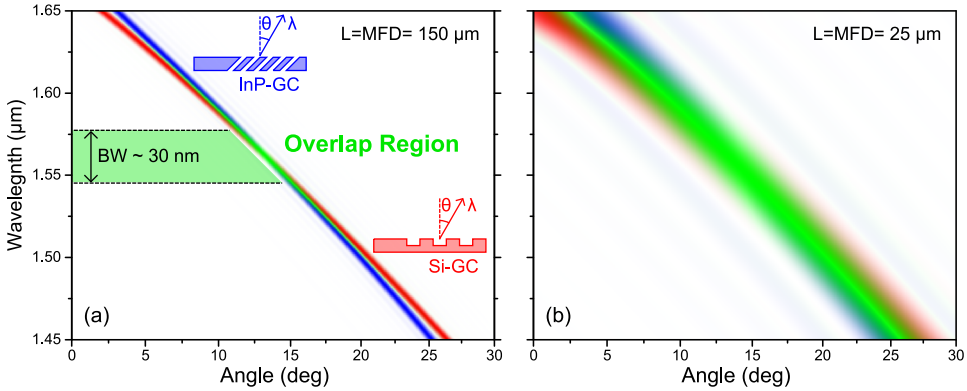

FIG. 6. Graphical representation of the far field projection's intensity for the 25 (a) and 150 (b) long grating as a function of the emission angle θ and wavelength λ. Both SOI (red) and InP (blue) are plotted in the same graph, and the overlap region is enlightened in green. Both profiles are normalized to the same maximum value for better visibility.

Furthermore, the far-field analysis could also provide insight on the fabrication and alignment tolerances. A variation from the optimal design could give a small shift or tilt in the emission profile. The wide overlap region of the shorter gratings makes them quite robust with respect to variations, while its shrinking as the gratings become longer gives an increased sensitivity. From Fig. 5 we estimate a $\pm 1^\circ$ tolerance on the emission angle for the 150 µm grating-couplers.

V. CONCLUSIONS

In summary, we analyzed the problem of grating-to-grating coupling between SOI- and InP-based platforms. We showed that by matching the scattering strengths between the two platforms, an insertion loss lower then 3dB with a useful bandwidth ($\approx$ 30 nm) can be reached. We optimized several designs with different lengths, to explore the trade-off between insertion loss and bandwidth/compactness. We notice that the present SOI- and InP-based structures are considerably different from previous grating couplers, as the need for optical matching between a high- and a low-index contrast grating imposes the use of chirped and unusually long gratings. Potential performance improvements could be achieved by customizing the layer thicknesses of the InP grating, opening the way to better directionality or greater scattering strength, allowing for lower insertion losses or more compact devices.

ACKNOWLEDGMENTS

We acknowledge Science Foundation Ireland (Grant number 12/RC/2276). We also thank Dr. Francisco Soares at Fraunhofer Heinrich Hertz Institute for useful discussions.

[1] L. Carroll, J.-S. Lee, C. Scarcella, K. Gradkowski, M. Duperron, H. Lu, Y. Zhao, C. Eason, P. Morrissey, M. Rensing *et al.*, Applied Sciences **6**, 426 (2016).
[2] A. Mekis, S. Gloeckner, G. Masini, A. Narasimha, T. Pinguet, S. Sahni, and P. De Dobbelaere, IEEE Journal of Selected Topics in Quantum Electronics **17**, 597 (2011).
[3] D. Vermeulen, S. Selvaraja, P. Verheyen, G. Lepage, W. Bogaerts, P. Absil, D. Van Thourhout, and G. Roelkens, Optics Express **18**, 18278 (2010).
[4] X. Chen, K. Xu, Z. Cheng, C. K. Fung, and H. K. Tsang, Optics Letters **37**, 3483 (2012).
[5] D. Benedikovic, C. Alonso-Ramos, P. Cheben, J. H. Schmid, S. Wang, D.-X. Xu, J. Lapointe, S. Janz, R. Halir, A. Ortega-Moñux *et al.*, Optics Letters **40**, 4190 (2015).
[6] A. Bozzola, L. Carroll, D. Gerace, I. Cristiani, and L. C. Andreani, Optics Express **23**, 16289 (2015).
[7] R. Marchetti, C. Lacava, A. Khokhar, X. Chen, I. Cristiani, D. J. Richardson, G. T. Reed, P. Petropoulos, and P. Minzioni, Scientific Reports **7**, 16670 (2017).
[8] S. Bernabé, C. Kopp, M. Volpert, J. Harduin, J.-M. Fédéli, and H. Ribot, Optics Express **20**, 7886 (2012).
[9] M. Cabezón, I. Garcés, A. Villafranca, J. Pozo, P. Kumar, and A. Kaźmierczak, Applied Optics **51**, 8090 (2012).
[10] G. Roelkens, L. Liu, D. Liang, R. Jones, A. Fang, B. Koch, and J. Bowers, Laser & Photonics Reviews **4**, 751 (2010).
[11] B. Corbett, R. Loi, W. Zhou, D. Liu, and Z. Ma, Progress in Quantum Electronics **52**, 1 (2017).
[12] N. Grote, M. Baier, and F. Soares, *Fibre Optic Communication* (Springer, 2017), pp. 799–840.

[13] M. Smit, X. Leijtens, H. Ambrosius, E. Bente, J. Van der Tol, B. Smalbrugge, T. De Vries, E.-J. Geluk, J. Bolk, R. Van Veldhoven *et al.*, Semiconductor Science and Technology **29**, 083001 (2014).
[14] H. H. I. Fraunhofer, "Foundry services on our photonic InP integration platform" (2016).
[15] J. Robinson and Y. Rahmat-Samii, IEEE Transactions on Antennas and Propagation **52**, 397 (2004).
[16] M. Passoni, D. Gerace, L. Carroll, and L. Andreani, Applied Physics Letters **110**, 041107 (2017).